Mecánica Computacional Vol. XXIV
A. Larreteguy (Editor)
Buenos Aires, Argentina, Noviembre 2005

DISPERSION PATTERNS IN A HETEROGENEOUS URBAN AREA

Fernando E. Camelli†, Rainald Löhner†, and Steven R. Hanna‡

†Laboratory for Computational Fluid Dynamics
George Mason University
Fairfax, Virginia, USA
email: fcamelli@gmu.edu, web page: http://www.scs.gmu.edu/fam

‡Hanna Consultants
Kennebunkport, Maine, USA

Key Words: Transport and dispersion of pollutants, CFD, LES.

Abstract. *A LES numerical modeling of flow in cities is presented. In three different scenarios, FEFLO-URBAN was used to analyze flow and dispersion patterns. First, a realistic urban setting in Tysons Corner, Northern Virginia, where the building geometry was obtained through blueprints; second, the MUST experiment conducted in the U.S. Army Dugway Proving Ground Horizontal Grid test site in Utah; and finally, a scenario in New York City as part of a collaborative effort supporting the design for the MSG05 Tracer experiment in the Madison Square Garden area.*

1 INTRODUCTION

The threat of an intentional chemical/biological/nuclear (CBN) release in a densely populated urban area has sparked research on dispersion patterns in urban scales for the last decade. The research on dispersion of gases for scales larger than a city has been the focus of study for decades now, and Gaussian models have been the most successfully applied to these large scales. Unfortunately, the simpler models have been unable to reproduce and capture all the complex processes at an urban level. The reason for this failure is primarily the inability to represent the mechanical forces (i.e. building geometry, trees, traffic) and the thermal forces (i.e. surface heating, HVAC systems) that control dispersion at this scale level. Dispersion models that use first principle physics are available today thanks to the sustained increase of computational ability to perform more operations in less time. This paper utilizes a Computational Fluid Dynamics (CFD) model called FEFLO-URBAN to accurately calculate in time the flow field inside an urban layout, incorporating the transport and dispersion of a passive release using an Eulerian framework. Three different scenarios will be presented: first, a realistic urban setting in Northern Virginia where the building geometry was obtained through blueprints (commercial development at Tysons Corner); second, the MUST experiment conducted in the U.S. Army Dugway Proving Ground Horizontal Grid test site in Utah; and finally, a scenario in New York City using FEFLO-URBAN as part of a collaborative effort supporting the design of the upcoming experiment in the Madison Square Garden area. The building geometry for New York City (NYC) was acquired from shape files facilitated by the Environmental Protection Agency. The set up of a simulation for a complex geometry like NYC requires a large number of man hours. In order to substantially reduce this time, an embedded approach was successfully applied.

2 MODEL DESCRIPTION

Atmospheric flow is mathematically modeled by the unsteady incompressible Navier-Stokes equations in 3D. Numerical solutions for these equations are obtained using FEFLO-URBAN, a multi-purpose finite element code[1]. Turbulence is modeled with LES using Smagorinsky closure[2]. The transport and dispersion equation is solved to simulate a passive scalar. To simulate building compounds, body-fitted and embedded[3] grid approaches are used.

2.1 Time integration

An explicit integration in time for the advective terms was used to capture the unsteadiness of the flow around the containers. Most of the diffusion in the atmosphere is due to the turbulent nature of the flow. The molecular diffusion is usually two orders of magnitude lower than the turbulent diffusion. Therefore, the time step selected for integration in time has to be small enough such that all the high frequencies that contribute to the turbulent diffusion are properly resolved in time. A projection scheme is used[4,5] with a multistage explicit advective prediction scheme[6].

2.2 Projection scheme

The equations describing incompressible, Newtonian flows are written as:

$$\frac{\partial \mathbf{v}}{\partial t} + \mathbf{v} \cdot \nabla \mathbf{v} + \nabla p = \nabla \mu \nabla \mathbf{v} \quad (1)$$

$$\nabla \cdot \mathbf{v} = 0 \quad (2)$$

Here *p* denotes the pressure, **v** the velocity vector and both the pressure *p* and the viscosity μ have been normalized by the (constant) density ρ . The important physical phenomena propagate with the advective timescales, i.e. with **v**. Diffusive phenomena typically occur at a much faster rate, and can/should therefore be integrated implicitly. Given that the pressure establishes itself immediately through the pressure-Poisson equation, an implicit integration of pressure is also required. The hyperbolic character of the advection operator and the elliptic character of the pressure-Poisson equation have led to a number of so-called projection schemes. The key idea is to predict first a velocity field from the current flow variables without taking the divergence constraint into account. In a second step, the divergence constraint is being separated into an advective-diffusive and pressure increment:

$$\mathbf{v}^{n+1} = \mathbf{v}^n + \Delta \mathbf{v}^a + \Delta \mathbf{v}^p = \mathbf{v}^\star + \Delta \mathbf{v}^p \quad (3)$$

For an explicit integration of the advective terms (with implicit integration of the viscous terms), one complete time-step is given by:

- Advective-Diffusive Prediction: $\mathbf{v}^n \rightarrow \mathbf{v}^\star$

$$\left[\frac{1}{\Delta t} - \theta \nabla \mu \nabla \right] (\mathbf{v}^\star - \mathbf{v}^n) + \mathbf{v}^n \cdot \nabla \mathbf{v}^n + \nabla p^n = \nabla \mu \nabla \mathbf{v}^n \quad (4)$$

- Pressure Correction: $p^n \rightarrow p^{n+1}$

$$\nabla \cdot \mathbf{v}^{n+1} = 0 \quad (5)$$

$$\frac{\mathbf{v}^{n+1} - \mathbf{v}^\star}{\Delta t} + \nabla \left(p^{n+1} - p^n \right) = 0 \quad (6)$$

which results in

$$\nabla^2 \left(p^{n+1} - p^n \right) = \frac{\nabla \cdot \mathbf{v}^\star}{\Delta t} \quad (7)$$

- Velocity Correction: $\mathbf{v}^n \rightarrow \mathbf{v}^\star$

$$\mathbf{v}^{n+1} = \mathbf{v}^\star - \Delta t \nabla \left(p^{n+1} - p^n \right) \tag{8}$$

At steady state, $\mathbf{v}^\star = \mathbf{v}^n = \mathbf{v}^{n+1}$ and the residuals of the pressure correction vanish, implying that the results do not depend on the time-step Δt. θ denotes the implicitness-factor for the viscous terms ($\theta = 1.0$: 1^{st} order, fully implicit, $\theta = 0.5$: 2^{nd} order, Crank-Nicholson). This scheme has been widely used in conjunction with spatial discretization based on finite differences[7–10], finite volumes[11], and finite elements[1,4,5,12,13].

3 STUDY OF THREE URBAN SETTINGS

3.1 Tysons Corner

The first urban setting is the commercial shopping center at Tysons Corner Virginia. The release of a passive substance was simulated. The first step in this simulation was to define the geometry of the set of buildings using a *computer aided design* (CAD) tool. The geometry has to be represented using analytical functions and/or discrete data. The surface representation has to be water tight, i.e. no holes, no overlapping, no gaps, or self intersections are allowed. The geometry description of Tysons Corner was constructed from a blueprint with the building distribution and the roof heights. This CAD process is not automatic in this particular case and it was tedious and time consuming. Depending on the geometrical complexity the CAD definition can be the most expensive part in any CFD process[14], with a great amount of man hours. There are attempts to make the CAD process automatic, e.g. using terrain and building height information from satellite images it is possible to reconstruct the topology by surface extrusion[15], or extraction of CAD information from photo images of buildings[16,17]. The lines and points for the Tysons Corner area are shown in Figure 1. The final CAD representation of Tysons Corner has 690 points, 1,077 lines, and 493 surfaces. Figure 2.(a) shows the surface of the computational domain and Figure 2.(b) shows the surface of the tetrahedral grid. The computational domain is 1,000 meters by 870 meters with a height of 325 meters. The final grid contains 187,376 triangles on the surface, 1,069,006 points, and 6,039,792 tetrahedra. The smallest size in the discretization is 0.22 meters and the largest size is 6.1 meters. The Tysons Corner example was run as incompressible and turbulent[5,18–21]. A logarithmic wind profile was used as incoming inflow, and the pressure was prescribed at the open boundaries of the computational domain. The normal velocity was set to zero on the walls and the law of the wall was applied. The pressure field is shown in Figure 3.(a), the velocity field in the wake of a building is in Figure 3.(b) and finally iso-surfaces of the level of concentration are shown in Figure 4.

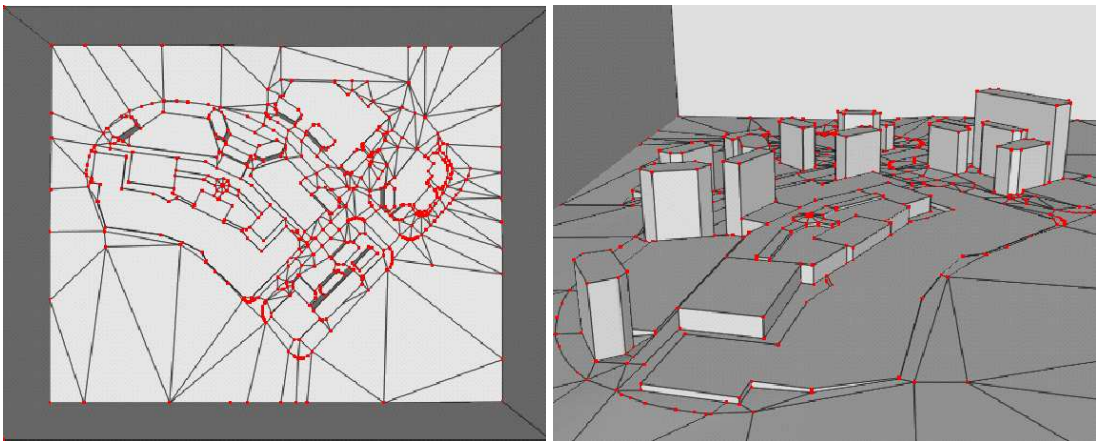

(a) Top view. (b) Side view.

Figure 1: CAD representation of Tysons Corner II.

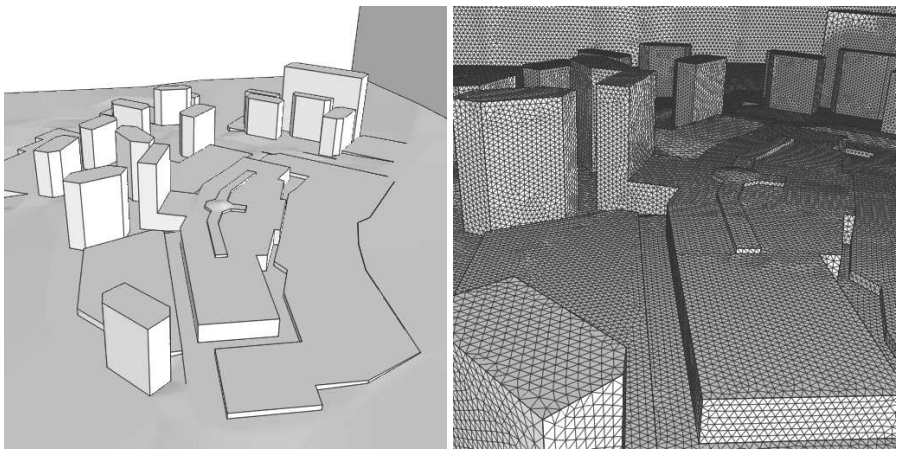

(a) Surface mesh shading. (b) Surface mesh.

Figure 2: Surface mesh of Tysons Corner II.

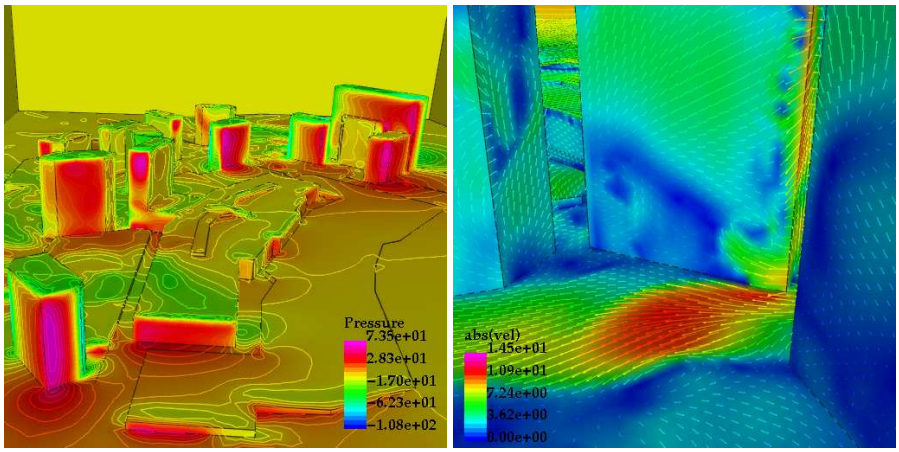

(a) Pressure distribution. (b) Velocity vectors.

Figure 3: Surface flow characteristics - Tysons Corner II.

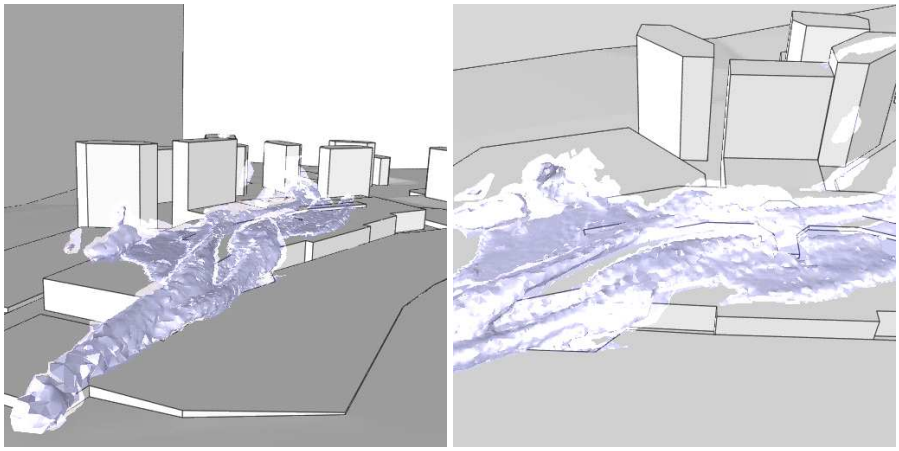

(a) View I (b) View II

Figure 4: Iso-surface of concentration - Tysons Corner II.

This example served to identify several issues that have been addressed in the last decade attempting realistic modeling of dispersion around buildings. Those issues include:

- automation and streamlining of the geometry definition process,
- enhancement of grid generation procedures that operate directly on discretely defined surfaces, i.e. triangulations,
- proper specification of time-dependent flow boundary conditions,
- proper modeling of turbulence effects,
- adequate mesh resolution to resolve small scale flow features and obtain accurate results,
- adequate time resolution, i.e. specification of optimum time-step sizes long enough to minimize CPU requirements but small enough to obtain an accurate solution,
- enhancement of data reduction procedures, e.g. to compute adequate time averages of turbulent flow quantities that can be directly compared to experimental measurements.

3.2 MUST experiment

The MUST experiment was designed to represent an urban layout with symmetric characteristics. An array of 10 by 12 containers was placed at the U.S. Army Dugway Proving Ground Horizontal Grid test site in Utah[22]. Each container was 12.2 m long, 2.42 m wide and 2.54 m high. The dimensions of the computational domain are: 320 m in length, 280 m in width, and 50 m in height above the ground. The MUST experiment utilized propylene as the tracer gas. The density of propylene (C_3H_6) is 1.769 kg/m^3. The tracer gas was measured using fast-response photo ionization detectors (PDI). The detectors were distributed between four 6 m towers, one 32 m tower, and four lines of sampling. The towers provided information of the vertical profile, while the sampling lines provided lateral dispersion information. Figure 5 shows the sensor distribution. A total of 72 stations were used within the array area. Four sampling lines with sensors at 1.6 m above ground were placed in the streets between containers. Reading from right to left in Figure 5:

1. sampling line 1: sensors 1 to 12,
2. sampling line 2: sensors 13 to 21,
3. sampling line 3: sensors 22 to 30,
4. sampling line 4: sensors 31 to 40.

Five towers with sensors were placed within the array area, one 32 m tower in the center and four 6 m towers located in each quadrant of the array. In addition to the information collected inside the array area, meteorological stations were placed outside the array to measure wind profiles and temperature. The MUST experiment produced 63 continuous releases and 5 trials with multiple puff releases. The experimental data was statistically analyzed to establish its quality. The trial 2682353 was selected because of its statistical quality. This case was a continuous release from the top of one of the container at a height of 5.2 m from the ground (see Figure 5).

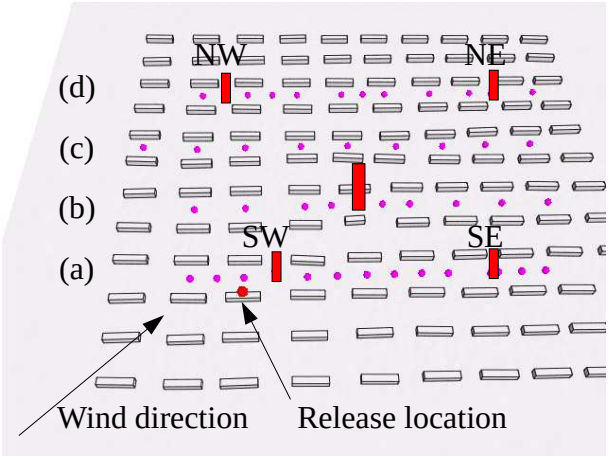

Figure 5: Source and station location.

The MUST simulation was carried out in four different volume meshes. The first has 576,411 elements (500K), the second has 3,988,500 elements (4M), the third has 8,267,552 elements (8M), and the fourth has 31,790,582 elements (31M). The average element size ranges from 0.64 m to 2.73 m (see Table 1).

Table 1: Mesh statistics

Nr. of elements	r_{min} [m]	r_{max} [m]	r_{mean} [m]
500K	0.54	19.23	2.73
4M	0.34	16.44	1.27
8M	0.18	16.96	0.88
31M	0.16	8.72	0.64

LES has shown limitations producing the right amount of turbulence close to the walls[23,24], therefore dispersion in the vicinity of walls is poorly predicted most of the time. In simple cases like a flat terrain, e.g. Prairie Grass experiment[25,26], the turbulence close to the surface is under-predicted and washed out in the vertical direction[27]. Hybrid RANS/LES methods give an

alternative[28] to circumvent this deficiency, but in some cases more resolution is required close to the surfaces. This not only increases the required number of elements, but also reduces the explicit time-step for time accurate integration. The computational domain is 325 meters by 280 meters with a height of 5 meters. The inflow wind profile was varying with time[29], in the rest of the open boundary the pressure was prescribed. The normal velocity was set to zero on the wall and the logarithmic law of the wall was applied.

The change of the concentration levels due to slightly different inflow wind directions is studied in the present section. This analysis is carried out with the mesh of 8.1M elements. Five different cases were run:

1. baseline case, with wind direction taken from the experiment;
2. a second case turning the wind direction 1° clockwise (CW) from the baseline wind direction;
3. a third case turning the wind direction 1° counter-clockwise (CCW) from the baseline wind direction;
4. a fourth case turning the wind direction 5° CW from the baseline wind direction;
5. and a fifth case turning the wind direction 5° CCW from the baseline wind direction.

In order to achieve a better quantification of the differences in concentration levels for different wind directions, a region of interest (ROI) is defined. This ROI is the area where the concentration level has surpassed or equaled a given threshold at any time during the elapsed 900 seconds of simulation. In other words, the ROI will cover an area where the concentration levels have exceeded, in some point in time, a pre-defined concentration level. Figures 6.a and 6.b show eight different snap-shots of the plume at a plane 1.5 m and 5.2 m above ground. These plume footprints enclose the area with concentration levels higher or equal to the threshold, i.e. 10^{-6} ppm, for eight different times. Figure 7 shows the resultant ROI's for the planes at 1.5 m and 5.2 m above the ground for the baseline case inflow direction. Figure 8.a shows the respective ROI's for clockwise and counter-clockwise rotation of the wind direction at the plane 1.5 m above ground. The dotted lines for each ROI represent the edges of the plume footprints. In Figure 8.b the overlapping of the previous four ROI's is presented. Clockwise edges are defined as the edges to the right when moving along the baseline wind direction, and counter-clockwise edges as the edges to the left when moving along the baseline wind. The clockwise edges of the five cases coincided. They are mostly aligned along the direction of the containers. The angle from the baseline direction to these edges is about 40°. In the counter-clockwise direction, the edges of the 1° CW, 1° CCW, and 5° CCW cases coincided again and they form an angle of 10° from the baseline wind direction. The counter-clockwise edge of the baseline case forms an angle of 6° from the baseline wind direction. The counter-clockwise edge of the 5° CW case forms an angle of less than 1° from the baseline wind direction. A channeling effect is observed for all five cases for the clockwise edges. The dispersion angle is augmented due to

the channeling[30]. The different wind directions have almost no effect in the dispersion angle on the clockwise direction.

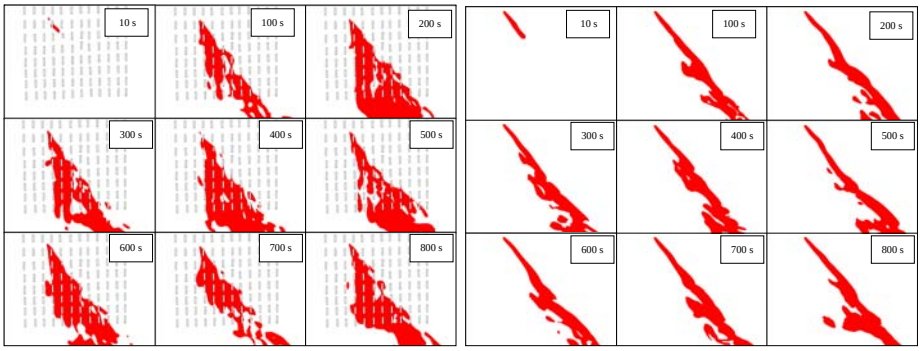

(a) Sequence of instantaneous plume footprints at 1.5 m above ground.

(b) Sequence of instantaneous plume footprints at 5.2 m above ground.

Figure 6: Sequence of instantaneous plume footprints.

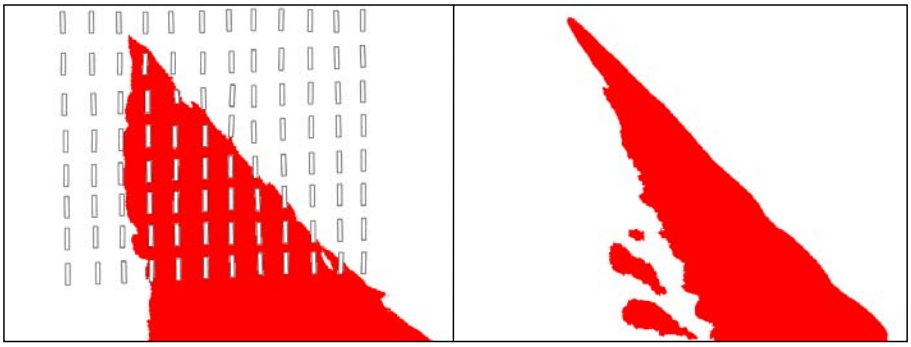

Figure 7: ROI's at 1.5 m (left) and 5.2 m (right) above the ground for the baseline case.

Figure 9.a shows the ROI's for the four cases at a height of 5.2 m above ground, which is the release height. The four plume footprints are overlapped in Figure 9.b. The plume clockwise edges coincided again and they form an angle of 30° from the baseline wind direction. Also the counter-clockwise edges coincided forming an angle of 12°. In all cases the plume shapes are not distinctively different, and the geometry of the array defines the shape. The channeling effect is obviously important and has to be considered. The 1° and 5° wind rotations do not have a large impact on the plume shape in the overall analysis.

A more detailed study should be conducted in order to consider different release heights, wind directions and geometry arrangements. In addition, the study should include large wind variations with respect to the baseline. Although this analysis is not conclusive, there is no indication that a small variation in the wind direction will produce large variation in the plume footprint.

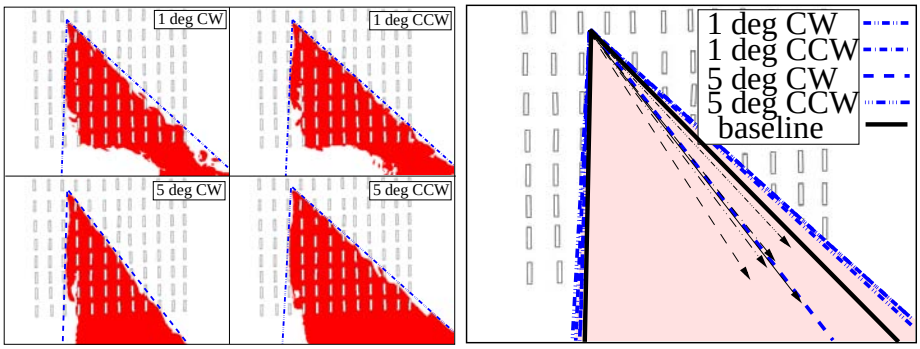

(a) ROI's at 1.5 m above ground.

(b) Overlap of the five ROI's at 1.5 m above ground.

Figure 8: ROI's at 1.5 m above ground.

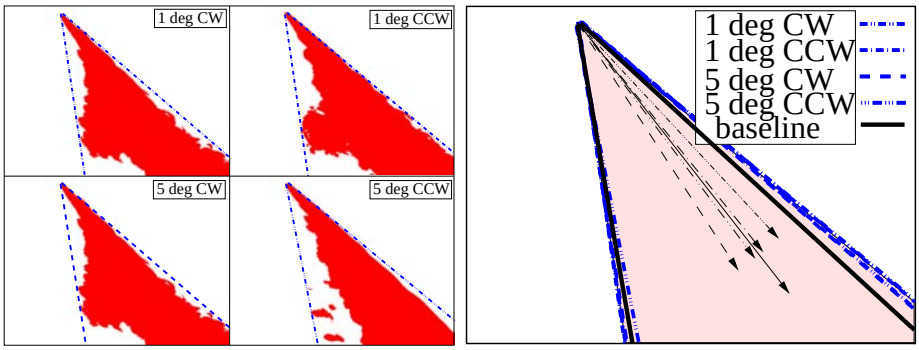

(a) ROI's at 5.2 m above ground.

(b) Overlap of the five ROI's at 5.2 m above ground.

Figure 9: ROI's at 5.2 m above ground.

3.3 New York City - Madison Square Garden

FEFLO-URBAN was used to simulate the Madison Square Garden Area as part of the planning for the MSG05 tracer experiment. A LES simulation was performed in a mesh of 24 millions of elements. The embedded^3 grid approach was used in the MSG simulation. This novel approach dramatically reduced the man-hours required for reconstructing the geometry of buildings as compared to the body-fitted approach. The area simulated was 4 square kilometers with a height of 600 meters. Winds from the SW and the WNW directions were simulated. A logarithmic profile was imposed as a boundary condition in the inflow in each case. The pressure was prescribed in the rest of the open boundaries. Figures 10 and 11 correspond to the simulation of wind from the SW. Figure 11 illustrates the air wake of the Empire State Building and the strong upward flow as a consequence of this tall building. This upward current can be observed with any tall building. The flow field produces a chimney effect in the downwind face of the building. Figure 11 depicts the flow around the MSG and the One Penn Plaza Building. Figures 11.a and 11.b show the wind vectors at 55 meters above ground level. Figure 11.c shows the vortices formed at the down wind face of the One Penn Plaza at 100 meters above ground level. Figure 11.d shows the flow at 5 meters above ground level.

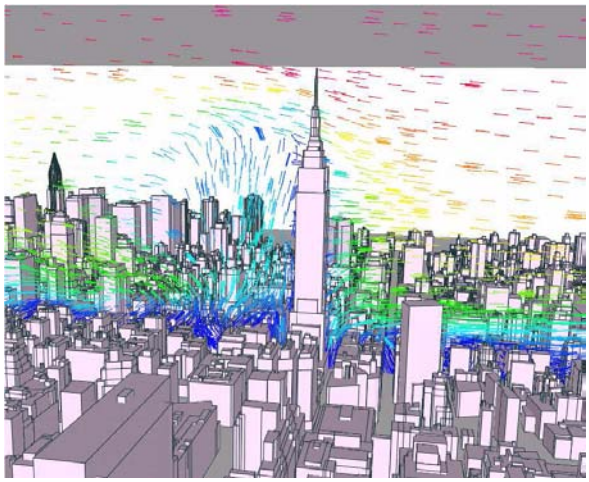

Figure 10: Empire State Building.

In the dispersion simulation, five near ground continuous releases were studied. Four releases were located at each corner of the MSG, and one at 34^{th} Street in front of the One Penn Plaza. For the release with the SW wind, 1800 seconds were integrated; and for the WNW wind, 1000 seconds. The release rates were of 1 gram per second with the SW wind, and 130 grams per second with the WNW wind. Figure 12 shows the plume of the five releases for 20, 500 and 1000 seconds with the SW wind. The plane shown in Figure 10 is at 14 meters above ground level. The plume shows a large dispersion in the direction transversal to the wind. The One Penn Plaza produced a large recirculation sending released material upwind from the release location.

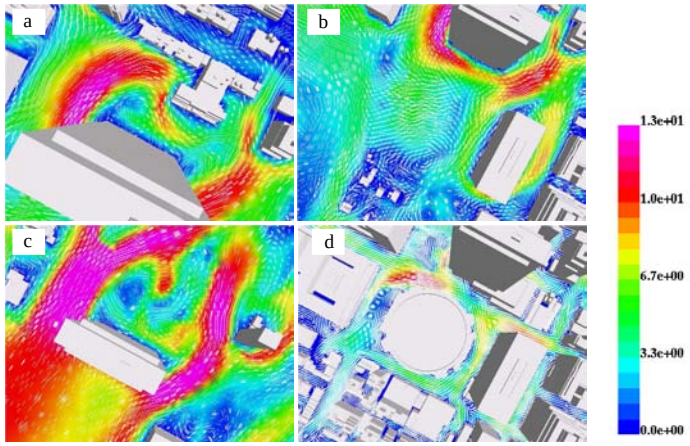

Figure 11: Velocity vectors at Madison Square Garden.

Figure 12: SW wind direction - Continuous release - Plume at 10, 500 and 1000 seconds.

Figure 13 shows the plume for the five releases at 20, 500 and 1000 seconds with the WNW wind. The lateral dispersion of this plume is narrower compared to the case of the SW wind. There is also a large recirculation in front of the Two Penn Plaza building that sends released material upwind from the release location. Some released material was channeled through Broadway Avenue.

An instantaneous release was simulated for the WNW wind condition. In this simulation the same five sources of the continuous release were used. The duration of this instantaneous release was of 300 seconds. Figure 14 shows the plume for the five releases at 20, 500 and 1000 seconds with WNW wind. The two first snapshots (20 and 500 seconds) are very similar to the ones for the continuous release (Figure 13). The snapshot that correspond to 1000 seconds shows how the level of concentration start to decrease in the far right end of the image.

The footprint of the plumes for the continuous releases with SW and WNW winds show very different dispersion rates in the lateral direction respect to the main wind direction. A large lateral dispersion on the SW wind direction is observed if is compared with the lateral dispersion of the WNW wind direction release. This augmentation in the lateral dispersion is due to the street orientation respect to the wind direction. If the wind is aligned with the streets (WNW wind direction), the lateral dispersion is not as large as in the case of a tilt of the streets

Figure 13: WNW wind direction - Continuous release - Plume at 10, 500 and 1000 seconds.

Figure 14: WNW wind direction - Puff release - Plume at 10, 500 and 1000 seconds.

orientations and wind direction (SW wind direction).

4 CONCLUSIONS

FEFLO-URBAN has been successfully tested and validated against problems of atmospheric dispersion for the past 10 years. The use of CFD tools has proved to be useful in the process of design planning for experiments (MSG05). The first two simulations, Tysons Corner Mall and the MUST experiment, were conducted using the body-fitted approach. This methodology requires a great deal of man-hours to be spent in the initial stages of any CFD simulation. The embedded grid approach greatly reduced the man hours expended to build the geometry of the MSG area. The FEFLO-URBAN simulation results of the MSG were part of preliminary studies for the MSG05 Tracer experiment, conducted in March, 2005. The use of CFD to study the possible scenarios previous to a field experiment was proved to be a success for the MSG tracer experiment. The knowledge of different plume footprints helped the distribution of resources on the ground. These series of simulations showed the effects of tall buildings (chimney effect) and the important relation between wind direction and street orientation for the lateral dispersion of the release material. Further simulations are been conducted for the second stage of the New York experiment. The final goal of this study is to compare the several CFD results among them and with the experimental data obtained during this field campaign.

REFERENCES

[1] R. Löhner. A fast finite element solver for incompressible flows. *AIAA Paper 1990-0398*, (1990).

[2] J. Smagorinsky. General circulation experiments with the primitive equations. I: The basic experiment. *Monthly Weather Review*, **91**, 99–165 (1963).

[3] R. Löhner, J. D. Baum, E. L. Mestreau, D. Sharov, C. Charman, and D. Pelessone. Adaptive embedded unstructured grid methods. *International Journal for Numerical Methods in Engineering*, **60**, 641–660 (2004).

[4] R. Löhner, C. Yang, E. Oñate, and S. Idelssohn. An unstructured grid-based parallel free surface solver. *Applied Numerical Mathematics*, **31**, 137–159 (1999).

[5] R. Ramamurti and R. Löhner. A parallel implicit incompressible flow solver using unstructured meshes. *Computers and Fluids*, **5**, 119–132 (1996).

[6] R. Löhner. Multistage explicit advective prediction for projection-type incompressible flow solvers. *Journal of Computational Physics*, **195**, 143–152 (2004).

[7] B. Alessandrini and G. Delhommeau. A multigrid velocity-pressure-free surface elevation fully coupled solver for calculation of turbulent incompressible flow around a hull. In *Porc. 21^{st} Symp. on Naval Hydrodynamics*, Trondheim, Norway, (June 1996).

[8] J. B. Bell and D. L. Marcus. A second order projection method for variable density flows. *Journal of Computational Physics*, **101** (1992).

[9] J. B. Bell, P. Colella, and H. Glaz. A second order projection method for the Navier-Stokes equations. *Journal of Computational Physics*, **85**, 257–283 (1989).

[10] J. Kim and P. Moin. Application of a fractional-step method to incompressible Navier-Stokes equations. *Journal of Computational Physics*, **59**, 308–323 (1985).

[11] Y. Kallinderis and A. Chen. An incompressible 3-D Navier-Stokes method with adaptive hybrid grids. *AIAA Paper 1996-0293*, (1996).

[12] K. J. Karbon and R. Singh. Simulation and design of automobile sunroof buffeting noise control. In *8^{th} AIAA-CEAS Aero-Acustics Conf.*, Breckenridge, (2002).

[13] E. Eaton. Aero-acoustic in an automotive HVAC module. In *American PAM User Conf.*, Birminghan, Michigan, (October 2001).

[14] R. Löhner. *Applied Computational Fluid Dynamics Techniques*. John Wiley & Sons, LTD, first edition, (2001).

[15] W. J. Coirier. Development of high fidelity pc based simulator for modeling the atmospheric transport and dispersion of nuclear, chemical, biological and radiological substances in urban areas. Phase I final report for DTRA, CFD Research Corp., (2001).

[16] S. M. Seitz and C. R. Dyer. Photorealistic scene reconstruction by voxel coloring. In *Proceedings of Computer Vision and Pattern Recognition Conference (CVPR97)*, pages 1067–1073, (1997).

[17] K. S. Roh and I. S. Kweon. 3-D object recognition using a new invariant relationship by single-view. *Pattern Recognition*, **33**, 741–754 (2000).

[18] J. R. Garratt. *The Atmospheric Boundary Layer*. Cambridge University Press, first edition,

(1994).
[19] S. P. Arya. *Introduction to Micrometeorology*. Academic Press, second edition, (1998).
[20] R. Löhner, K. Morgan, J. Peraire, and M. Vahdati. Finite element flux-corrected transport (FEM-FCT) for Euler and Navier-Stokes equations. *International Journal for Numerical Methods in Fluids*, **7**, 1093–1109 (1987).
[21] O. Soto, R. Löhner, and J. R. Cebral. An implicit monolithic time accurate finite element scheme for incompressible flow problems. *AIAA Paper 2001-2616*, (2001).
[22] C. A. Biltoft. Abbreviated test plan for customer test: Mock urban setting test (MUST). DPG Document WDTC-TP-01-028, Defense Threat Reduction Agency, (2001).
[23] P. J. Mason. Large-eddy simulation: A critical review of the technique. *Journal of the Royal Meteorology Society*, **120**, 1–16 (1994).
[24] U. Piomelli. Large-eddy simulation: Achievements and challenges. *Progress in Aerospace Science*, **35**, 335–362 (1999).
[25] M. L. Barad. Project Prairie Grass, a field program in diffusion. *Journal of Geophysical Research*, **1–2** (1958). Report AFCRC-TR-58-235, U.S. Air Force Cambridge Research Center.
[26] D. A. Haugen. Project prairie grass, a field program in diffusion. *Journal of Geophysical Research*, **3** (1959). Report AFCRC-TR-58-235, U.S. Air Force Cambridge Research Center.
[27] F. Camelli and R. Löhner. Flow and dispersion around buildings: An application with FEFLO. In *Proc. for ECCOMAS 2000, European Congress on Computational Methods*, Barcelona, Spain, (September 2000).
[28] F. Camelli and R. Löhner. Combining the Baldwin-Lomax and Smagorisky turbulence models. *AIAA Paper 2002-0426*, (2002).
[29] S. R. Hanna, S. Tehranian, B. Carissimo, R. W. Macdonald, and R. Löhner. Comparisons of model simulations with observations of mean flow and turbulence within simple obstacle arrays. *Atmospheric Environment*, **36**(32), 5067–5079 (2002).
[30] B. Carissimo. Preliminary numerical simulations of the mock urban setting test (MUST). In 5^{th} *Annual George Mason University Transport and Dispersion Modeling Workshop*, Fairfax, VA, (July 2001).